ELSEVIER

Contents lists available at ScienceDirect

International Journal of Refractory Metals and Hard Materials

journal homepage: www.elsevier.com/locate/IJRMHM





Mechanical properties of molybdenum containing MoO_2 and HfO_2 processed by field assisted sintering technology (FAST): Characterization and modeling

Erik T. Furton ^a, Patrick E. Albert ^{a,b}, Dax H. Hoffman ^a, Douglas E. Wolfe ^{a,b,c,d}, Allison M. Beese ^{a,e,*}

- ^a Department of Materials Science and Engineering, The Pennsylvania State University, University Park, PA 16802, United States
- ^b Applied Research Laboratory, The Pennsylvania State University, University Park, PA 16802, United States
- ^c Department of Engineering Science and Mechanics, The Pennsylvania State University, University Park, PA 16802, United States
- d Ken and Mary Alice Lindquist Nuclear Engineering Department, The Pennsylvania State University, University Park, PA 16802, United States
- e Department of Mechanical Engineering, The Pennsylvania State University, University Park, PA 16802, United States

ARTICLE INFO

Keywords:
Molybdenum
Field-assisted sintering technology
Hafnium oxide
Three-point bending
Bilinear constitutive model

ABSTRACT

Molybdenum and its alloys are of interest for applications with extreme thermomechanical requirements such as nuclear energy systems, electronics, aerospace vehicles, and hypersonic vehicles. In the present study, pure molybdenum and samples with added hafnium carbide (HfC) grain refiners were produced using field assisted sintering technology (FAST). The molybdenum and HfC reacted with oxygen to produce MoO_2 and HfO_2 , and increased HfC content from 1 wt% to 5 wt% decreased grain size while the microhardness correspondingly increased. Room temperature three-point bending tests were conducted, and finite element modeling was used to define HfC-dependent bilinear material models. The presence of oxygen most severely affected pure molybdenum, which exhibited little strength and limited ductility, whereas for samples with added HfC, HfO_2 was present, resulting in increased toughness hypothesized to be due to microcrack toughening. The samples with 1 wt% added HfC had the greatest energy absorption capability.

1. Introduction

Molybdenum has one of the highest melting points for any element, at 2620 °C, making it appealing for extreme applications such as furnace lining, nuclear power production, tooling for hot forming, and the emerging field of hypersonic vehicles [1–3]. Although the latter is associated with extreme temperatures, oxidizing environments, and high stresses, auxiliary components are subject to less severe restrictions but may have additional considerations such as high thermal or electrical conductivity [4].

Molybdenum has limited ductility at room temperature, largely due to grain boundary embrittlement by oxygen [5,6]. Molybdenum oxide (MoO₂) preferential forms along grain boundaries and causes brittle intergranular fracture. To mitigate grain boundary impurities, either the starting material may be reduced or oxygen absorbing additives such as zirconia, carbon, tungsten, rhenium, hafnium carbide, or carbon may reduce MoO₂, thereby increasing mechanical strength [1,7–9].

One method for increasing the ductility, high temperature strength, fracture toughness, and creep resistance of metal matrices is through the addition of dispersed oxide or carbide particles, referred to as oxide dispersion-strengthened (ODS) and carbide dispersion-strengthened (CDS) alloy systems, respectively [10-12]. The incoherent oxide and carbide particles, often tailored for the lattice mismatch or strain energy at the interface between the particles and the refractory metal matrix, result in improved strength and toughness by increasing the overall interfacial energy. This engineered interface acts as a barrier for dislocation movement and thus improves strength. In addition, dispersion strengthening results in superior thermal stability due to an increase in recrystallization temperature that can be attributed to the pinning of grain boundaries and dislocations. The hardness enhancements due to grain boundary pinning are associated with the ability to maintain a fine-grained microstructure and the Hall-Petch relationship. Various oxides and carbides such as Y₂O₃, MoO₂, HfO₂, La₂O₃, CeO₂, ZrO₂, HfC, TaC, TiC, ZrC, and B₄C can be used depending on the alloy matrix crystal

^{*} Corresponding author at: Department of Materials Science and Engineering, The Pennsylvania State University, University Park, PA 16802, United States. E-mail address: beese@matse.psu.edu (A.M. Beese).

structure and properties of interest, with the volume fraction, homogeneity and particle size contributing to the mechanical properties of interest $\lceil 13-18 \rceil$.

In addition to improving mechanical properties through grain-boundary engineering, a dispersion of hard particles can also increase a material's toughness through microcrack toughening [17,19,20]. Microcrack toughening occurs when microscopic cracks initiate at particle-matrix interfaces and are arrested as the crack is absorbed or deflected before causing catastrophic failure. The microcracks accommodate expansion, relieving local tensile stresses. Once a critical stress is reached where cracks initiate, the material's stiffness is reduced [19]. This mechanism, while superficially resembling strain hardening, cannot be described by strain hardening constitutive equations.

Due to the high melting points of pure molybdenum and its alloys, it is challenging to fabricate near net shape components with high density and tailored microstructures. As such, powder processing methods are preferred relative to forming or casting. Liquid sintering aids such as nickel and copper have been used to increase density, but the formation of brittle, low melting temperature intermetallic phases limits its applicability [21]. Similarly, the use of sintering aids, while increasing density and strength at room temperature, precludes application in high-temperature environments.

Field-assisted sintering technology (FAST) is a processing method capable of rapidly manufacturing complex near net shape geometries [22,23]. FAST uses an electrically conductive die assembly, traditionally graphite, that is biased with high current, low voltage pulsed DC waveforms to provide field-assisting mechanisms that accelerate sintering processes [24]. Joule heating allows for the avoidance of the long ramp times and conduction-limited heat transfer rates associated with traditional sintering techniques, and densification is further aided due to additional localized heating in the vicinity of defects, yielding neartheoretical densities with minimal grain growth. Pure molybdenum has been densified to near theoretical densities through FAST, although excessive sintering times and temperatures can lead to increased grain size and reduced strength [25,26].

In this study, nominally pure molybdenum and three compositions containing $Mo_{1-x}(HfC)_x$ were fabricated and characterized by Archimedes density measurements, scanning electron microscope (SEM) imaging, and X-ray diffraction (XRD). Room-temperature three-point bending tests were conducted to identify the impact of the added HfC on the mechanical behavior of the materials. Through comparison to experiments, corresponding finite element simulations were used to calibrate composition-dependent parameters for bilinear constitutive models. Due to the presence of oxygen during sintering, increasing the added HfC concentration increased the ratio of HfO₂ to MoO_2 , which resulted in improved mechanical properties. Only the nominally pure molybdenum did not meet the tensile strength requirement of 585 MPa for pure molybdenum [27], and the samples containing 1% added HfC reached the greatest strain energy density prior to fracture.

2. Material and methods

2.1. Powders

Pure molybdenum and three compositions of $Mo_{1-x}(HfC)_x$ were prepared, where x ranged between 1 wt% and 5 wt% as shown in

Table 1
Compositions of Mo_{1-x}(HfC)_x samples.

| Sample | Мо | | HfC | | # Samples |
|--|------|------|-----|------|-----------|
| | Wt% | Mol% | Wt% | Mol% | |
| Мо | 100 | 100 | 0.0 | 0.0 | 2 |
| $Mo_{0.99}(HfC)_{0.01}$ | 99.0 | 99.5 | 1.0 | 0.5 | 2 |
| $Mo_{0.97}(HfC)_{0.03}$ | 97.0 | 98.5 | 3.0 | 1.5 | 2 |
| Mo _{0.95} (HfC) _{0.05} | 95.0 | 97.4 | 5.0 | 2.6 | 3 |

Table 1. The molybdenum powder (10.2 g/cm³) (Atlantic Equipment Engineering, Inc., Upper Saddle River, NJ) had 99.8% purity and was manufactured via hydrogen reduction with average particle size ranging from 1 μ m to 5 μ m. The hafnium carbide powder (12.2 g/cm³) (Reade Advanced Materials, Newton, MA) had a purity of 99% with average particle diameters between 1 μ m and 3 μ m.

X-ray diffraction (Empyrean III, Malvern PANalytical, Malvern, United Kingdom) was performed on the as-received powders to identify impurities. $\text{CuK}\alpha$ radiation (1.5406 Å) with a nickel filter, operating voltage of 45 kV, and a current of 40 mA was used in a Bragg-Brentano geometry with a 2 mm by 6 mm mask size. XRD scans on the mechanical test samples (discussed in Section 2.4) used the same parameters as the powders, except that the mask size was restricted to 0.3 mm by 0.4 mm to ensure the beam scanned only the sample. Phase identification was performed using JADE (International Centre for Diffraction Data, Newtown Square, PA).

The molybdenum powder, in addition to the body centered cubic (BCC) molybdenum phase, also contained MoO_2 in trace quantities (Fig. 1a). The MoO_2 in the starting bulk powders can readily segregate to grain boundaries during processing [28,29]. The as-received hafnium carbide powder also contained trace amounts of monoclinic HfO_2 (Fig. 1b).

The HfC powder was attrition milled with 2 mm yttrium stabilized zirconia (YSZ) ball media in isopropyl alcohol (IPA) for 3 h to reduce the particle size, then dried at atmosphere for 24 h at 100 °C to remove the IPA prior to blending with the molybdenum. The molybdenum and hafnium carbide powders were then blended in high density polyethylene (HDPE) bottles for 4 h using 3/16" tungsten carbide (WC) satellite media at a 4:1 ball-to-powder mass ratio. After the powders were prepared using their respective milling techniques, XRD did not identify any new phases or significant changes in oxide peak intensities.

2.2. FAST processing

Samples were manufactured with a 25-ton FAST system (FCT Systeme GmbH, Frankenblick, Germany). The powders were pressed in a graphite die with a diameter of 40 mm to produce a 5 mm tall sample (Fig. 2). Prior to sintering, the die set was lined with graphite foil to prevent damage or contamination to the mold and assist in sealing the space between die components. The chamber was then evacuated to a base pressure of approximately 500 Pa, which limited oxidation. Preliminary pure molybdenum pucks were manufactured to determine optimal FAST processing parameters to achieve nearly fully dense samples without excessive grain growth. Subsequent samples, including those with HfC grain refiners, were fabricated with 100 °C/min sintering ramp rates from room temperature to the soak temperature, and an applied uniaxial compressive stress of 70 MPa. The samples were held at 1750 °C for 20 min before vacuum cooling to room temperature. Prior to subsequent characterization and mechanical testing, the sample surfaces were mechanically ground to remove a brittle carbide layer, which formed due to carbon diffusion from the graphite foil during processing [25].

2.3. Characterization

The Archimedes method was used to measure density of the pucks, with a digital scale (Explorer, OHAUS, Parsippany–Troy Hills, NJ). All samples had densities between 97%–99% (Table 2). For microstructural examination, samples were mounted in epoxy and polished to a mirror finish using 1 μ m polycrystalline diamond in the final step. Cross-sections were imaged with scanning electron microscopy in back-scattered electron mode; prior to mechanical testing, material was etched with Murakami's reagent to increase phase contrast (Mira 3, TESCAN, Brno, Czech Republic), and after fracture, the material was not etched to identify crack networks near the fracture surfaces (Apreo S, ThermoFisher Scientific, Waltham, MA).

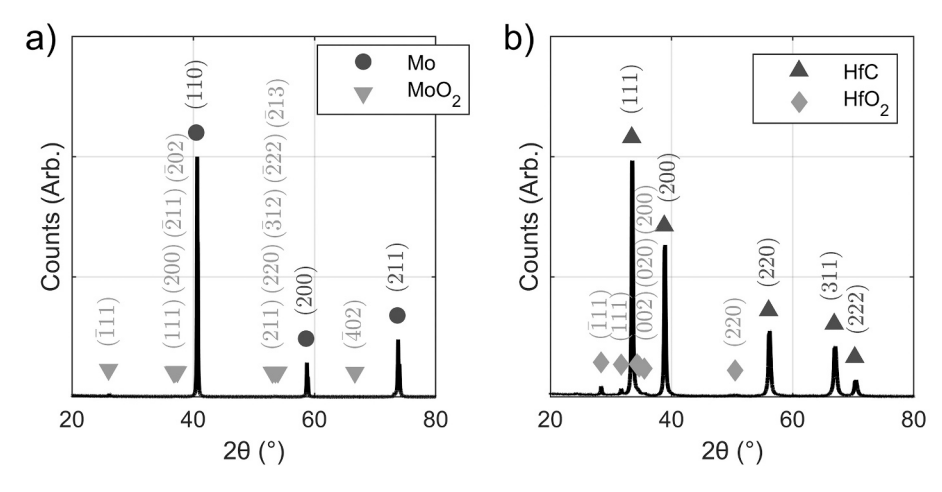


Fig. 1. X-ray diffraction of (a) molybdenum and (b) hafnium carbide powders. Each powder was shown to contain trace amounts of oxides.

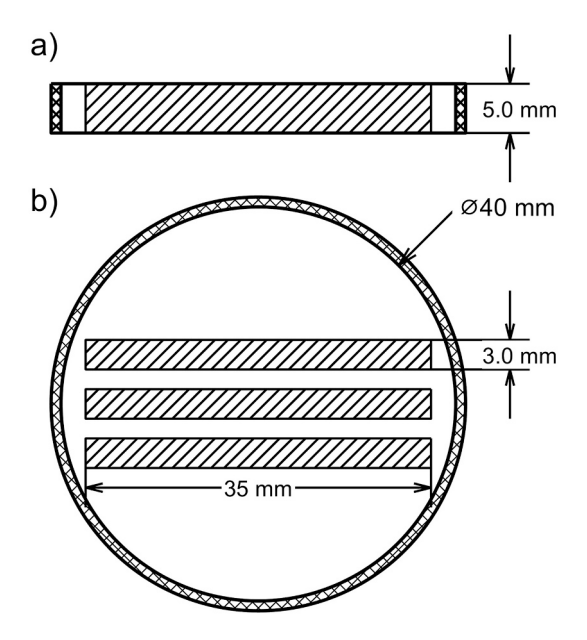


Fig. 2. (a) Side-view and (b) top-view of pucks fabricated by FAST along with mechanical test specimens. The puck was surrounded by a graphite foil, pictured with a double crosshatch and with exaggerated thickness for clarity. Mechanical test specimens were cut from the puck for 3-point bending (shaded with a single crosshatch).

Table 2Archimedes densities of samples produced by FAST, where the uncertainty is reported as one standard deviation. The theoretical density was calculated by the rule of mixtures using the compositions in Table 5.

| Sample | Density (%) | Theoretical Density (g/cm ³) |
|-------------------------|------------------|--|
| Мо | $98.4 \pm 0.2\%$ | 10.05 |
| $Mo_{0.99}(HfC)_{0.01}$ | $98.8\pm0.1\%$ | 10.11 |
| $Mo_{0.97}(HfC)_{0.03}$ | $98.0\pm0.1\%$ | 10.23 |
| $Mo_{0.95}(HfC)_{0.05}$ | $98.3\pm0.1\%$ | 10.22 |

The oxygen contents of the pucks were measured with the inert gas fusion method (IMR Test Labs, Lansing, NY) and are presented in Table 3. To identify the effect of oxygen content, equilibrium phases were calculated using thermodynamic modeling with the CALPHAD (CALculation of PHAse Diagrams) approach (Thermo-Calc 2016b, Sweden) with a molybdenum-hafnium-carbon database appended to the SGTE 5.0 database [30]. The former database considered the

Table 3 Measured and calculated starting oxygen content. The measured concentration was obtained with the inert gas fusion method, and the starting concentration is the amount of oxygen initially required in the system at 1750 $^{\circ}$ C to produce a solid containing the measured oxygen concentration.

| Sample | Starting Concentration | Measured Concentration |
|--|------------------------|------------------------|
| Мо | 0.87% | 0.87% |
| $Mo_{0.99}(HfC)_{0.01}$ | 0.91% | 0.80% |
| $Mo_{0.97}(HfC)_{0.03}$ | 1.00% | 0.67% |
| Mo _{0.95} (HfC) _{0.05} | 0.95% | 0.84% |

solubility of carbon in molybdenum, while it was assumed that all oxygen-containing compounds had zero solubility. Some of the initial oxygen content formed gaseous products that were removed from the system, while the remainder formed solid oxide phases in the samples, and their oxygen content was measured with the inert gas fusion method (Table 3). The starting oxygen content which results in the measured oxygen content of solid material at 1750 °C was calculated and used in subsequent analyses.

The ASTM E112 intercept procedure was used to identify grain size [31]. Microhardness measurements were conducted with a Vickers diamond indenter (LM110AT, Leco, St. Joseph, MI) in accordance with ASTM C1327 [32]. For each composition, 15 indents were made, using 100 g-force with a dwell time of 10 s.

2.4. Mechanical testing

For three-point bending mechanical testing, three samples were cut from each puck with a 5'' diamond blade on a wafering saw, with dimensions of 5 mm \times 3 mm \times 35 mm (Fig. 2). The samples were polished with 1200 grit silicon carbide to remove cutting damage and ensure fracture was not initiated by surface roughness, with the grinding parallel to the sample's longitudinal axis to reduce stress concentrations [33]. The cross-sectional sample dimensions after grinding and polishing are tabulated in Table 4.

Three-point bending was conducted using a universal load frame (Criterion 43, MTS Systems, Eden Prairie, MN) with a crosshead displacement rate of 0.005 mm/s, a distance between outer pins of 30 mm, and pin diameters of 2.0 mm. Displacement was measured using digital image correlation (DIC), a non-contact method for measuring surface deformation. The mechanical testing samples were painted with a random black speckle pattern overlaid on a white basecoat. During mechanical testing, images were captured at a frequency of 1 Hz with a digital camera (GRAS-50S5M-C, Teledyne FLIR, Wilsonville, OR), and the deflection of the sample's center relative to the outer pins was calculated by tracking the deformation of the speckle pattern with DIC

Table 4

Mean sample dimensions for mechanical testing. Samples labeled with an asterisk were excluded from further analysis due to large macroscopic defects.

| | Sample #1 | | Sample #2 | | Sample #3 | |
|--|------------|-------------------|------------|-------------------|------------|-------------------|
| | Width (mm) | Thickness (mm) | Width (mm) | Thickness (mm) | Width (mm) | Thickness (mm) |
| Мо | 2.04* | 1.94* | 3.16 | 1.87 | 2.29 | 2.12 |
| $Mo_{0.99}(HfC)_{0.01}$ | 4.45 | 2.38 | 4.24* | 2.11* | 4.29 | 2.35 |
| $Mo_{0.97}(HfC)_{0.03}$ | 4.41* | 3.01* | 4.31 | 2.88 | 4.21 | 2.20 |
| Mo _{0.95} (HfC) _{0.05} | 4.35 | 2.28 | 4.34 | 2.42 | 4.35 | 2.49 |

software (VIC-2D, Correlated Solutions, Imro, SC).

The fracture surfaces were imaged with optical microscopy (VHX-2000, Keyence, Osaka, Japan). Three samples, each of different composition, were excluded from the mechanical test results because their fracture surfaces contained large, macroscopic processing defects. The total number of non-excluded samples are shown in Table 1.

To identify an appropriate constitutive relationship for the materials, each mechanical test was simulated with three-dimensional finite element simulations (Abaqus, Dassault Systèmes, France). The simulations' cross-sections were modeled after optical micrographs of the fracture surfaces, and all elements were C3D8 full-integration bricks with the smallest element length of 200 μ m. Agreement between experiments and simulations was not possible using a typical strain hardening model, such as the Swift hardening law, except for pure molybdenum. Instead, the nonlinear mechanical behavior was best described by a bilinear constitutive equation:

$$\overline{\sigma} = \begin{cases} E\overline{\varepsilon} \, for \, \overline{\sigma} \le \sigma_P \\ \sigma_P(1-\alpha) + \alpha E\overline{\varepsilon} \, for \, \overline{\sigma} > \sigma_P \end{cases}$$
(1)

where $\overline{\sigma}$ is the von Mises equivalent stress, $\overline{\epsilon}$ is the total von Mises equivalent strain, and E is the Young's modulus. It was assumed that E=324 GPa for all compositions, and the Poisson ratio was 0.29 [34]. The parameter σ_p is the stress at the onset of nonlinearity, or the stress at which the linear stress-strain slope decreases as observed in materials that develop microcracking during loading [35]. The parameter α is the ratio of the secondary stress-strain slope to the initial modulus.

Force-displacement behavior from finite element simulations is

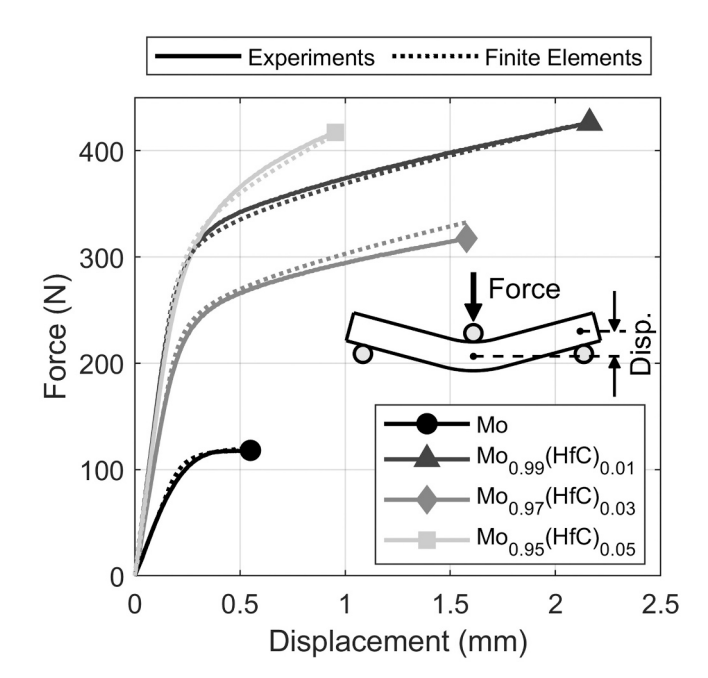


Fig. 3. Representative force-displacement behavior for three-point bending. The finite element simulations were terminated at the experimentally determined failure displacements.

compared to experimental force-displacement behavior in Fig. 3. In the elastic region, large differences in the flexural modulus were caused by differences in sample thickness (Table 4). The fact that a bilinear constitutive relationship was required to capture the observed experimental data suggests the hypothesis that the nonlinear behavior is due to microcrack toughening rather than strain hardening.

3. Results and discussion

3.1. FAST processing

In the nominally pure molybdenum sample, in addition to BCC molybdenum, XRD identified MoO₂, as shown in Fig. 4a; MoO₂ particles are labeled in the SEM micrograph in Fig. 5a. Thermodynamic modeling, as shown in Fig. 6a, identified that all oxygen would form MoO₂. Furthermore, for a composition of pure molybdenum with 0.87 wt% oxygen (Table 3), the isopleth in Fig. 6e shows that a processing temperature of 1750 °C was insufficient to decompose the MoO₂.

For samples with between 1% and 3% added HfC, two populations of particles were visible in the SEM micrographs in Fig. 5b-c. Thermodynamic simulation results in Fig. 6b-c indicated that the presence of oxygen would deplete all the HfC and produce HfO₂:

$$2Mo + O_2 + HfC \rightarrow Mo_2C + HfO_2, \tag{2}$$

During processing, at approximately 1070 °C, the Mo₂C decomposes:

$$MoO_2 + 2Mo_2C \rightarrow 5Mo + 2CO$$
, and

$$MoO_2 + Mo_2C \rightarrow 3Mo + CO_2 \tag{3}$$

as shown in Fig. 6f-g. With both compositions, Mo₂C was the limiting reactant and only MoO₂ remained. At approximately 1830 °C, HfO₂ undergoes a phase transformation, where during cooling the tetragonal phase transforms to monoclinic phase, and the volume increases by approximately 3% [36]. This allotropic transformation has been documented to cause microcrack toughening in other material systems [36]. Although the transformation temperature of 1830 °C exceeds the nominal processing temperature of 1750 °C, in FAST the local temperature at discontinuities, such as the particle-matrix interface, exceeds the far-field temperature [23].

For samples with 5 wt% added HfC, an oxygen concentration of 0.95 wt% eliminates all HfC. The reaction in $\it Eq.~3$ consumes all MoO₂, leaving behind Mo₂C, as shown in Fig. 6h. Peaks from both phases are identified in XRD in Fig. 4d and the phases are identified in the micrograph in Fig. 5d.

As a summary, the equilibrium weight fractions of the various oxides and carbides at a processing temperature of 1750 $^{\circ}$ C are shown in Table 5. For all samples, all the initial HfC was depleted. Increasing the amount of added HfC increased the ratio of HfO₂ to MoO₂.

The mean grain size decreased with increasing HfC concentration as shown in Fig. 7. The Vickers hardness correspondingly increased in a Hall-Petch manner [37,38], where HV_0 is the Vickers hardness for a material without grain boundaries and d the mean grain size:

$$HV = HV_0 + k/\sqrt{d} \tag{4}$$

Assuming that grain size was the only factor that affected hardness,

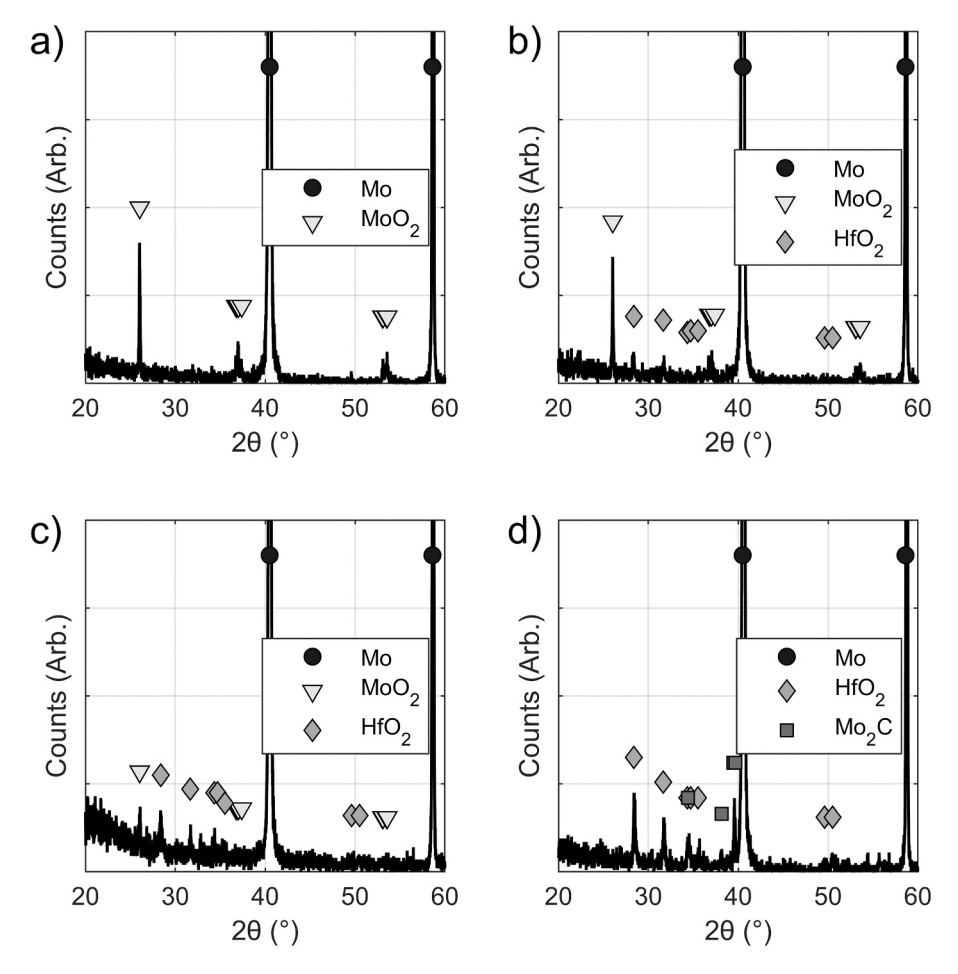


Fig. 4. X-ray diffraction of sintered (a) pure molybdenum, (b) $Mo_{0.99}(HfC)_{0.01}$, (c) $Mo_{0.97}(HfC)_{0.03}$, and (d) $Mo_{0.95}(HfC)_{0.05}$. The molybdenum peaks are cut off for clarity.

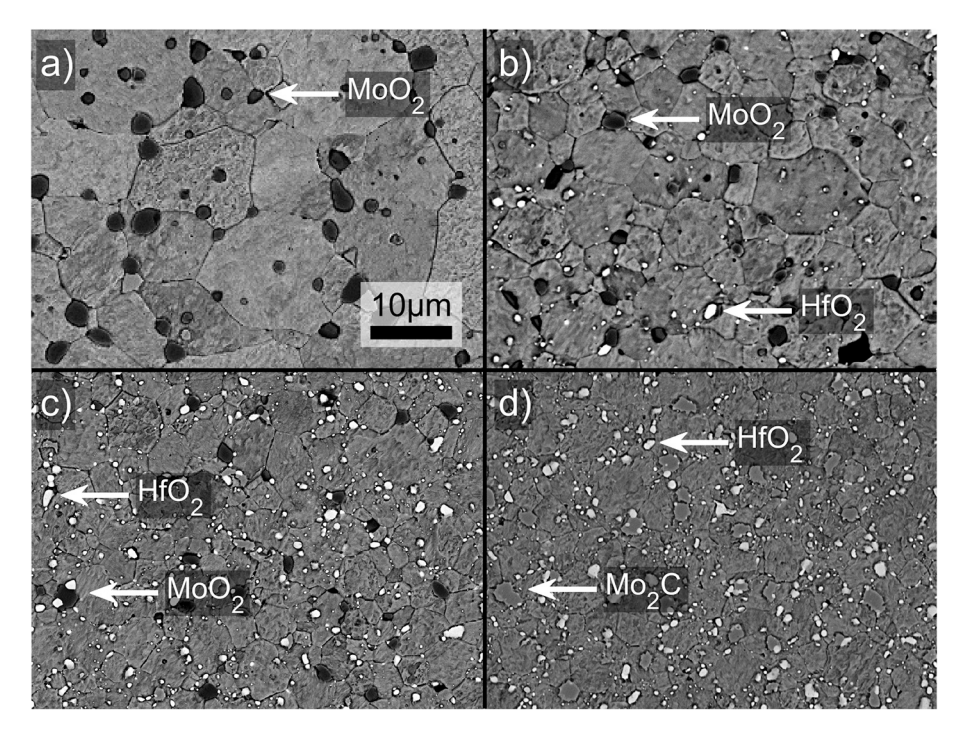


Fig. 5. SEM micrographs of (a) molybdenum sample, and (b) $Mo_{0.99}(HfC)_{0.01}$, (c) $Mo_{0.97}(HfC)_{0.03}$, and (d) $Mo_{0.95}(HfC)_{0.05}$. Representative particles of MoO_2 , HfO_2 , and Mo_2C are labeled.

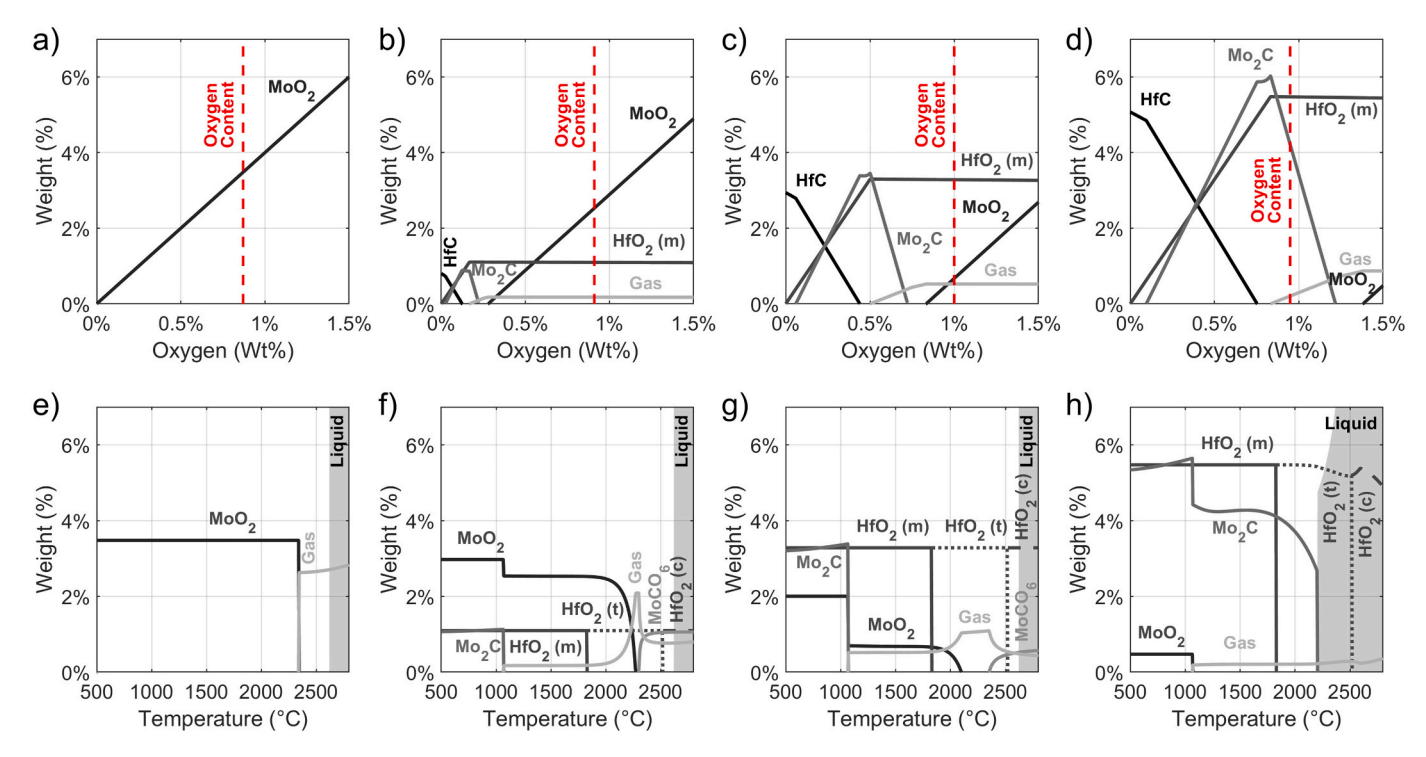


Fig. 6. Computationally predicted weight fractions of thermodynamically stable phases as function of oxygen concentration at 1750 °C for (a) Mo, (b) $Mo_{0.99}(HfC)_{0.01}$, (c) $Mo_{0.97}(HfC)_{0.03}$, and (d) $Mo_{0.95}(HfC)_{0.05}$ compositions. The y-axis corresponds to the weight fraction, y, for $(Mo_{1.x}(HfC)_x)_{1.y}O_y$. The vertical dashed lines represent the starting oxygen content from Table 3. Isopleths with starting oxygen content for (e) Mo, (f) $Mo_{0.99}(HfC)_{0.01}$, (g) $Mo_{0.97}(HfC)_{0.03}$, and (h) $Mo_{0.95}(HfC)_{0.05}$ compositions. The shaded regions represent the liquid phase. The balance for each subfigure is metallic molybdenum. The three allotropes of HfO_2 are labeled: monoclinic (m), tetragonal (t), and cubic (c).

Table 5 Thermodynamic calculations for weight fractions of oxide and carbide phases in solid material at a temperature of 1750 $^{\circ}$ C and a pressure of 1 atm with oxygen content as shown in Table 3.

| Starting Composition | MoO ₂ (Wt%) | HfO ₂ (Wt%) | Mo ₂ C (Wt%) |
|--|---------------------------|---------------------------|----------------------------|
| Мо | 3.5% | - | - |
| $Mo_{0.99}(HfC)_{0.01}$ | 2.5% | 1.1% | _ |
| Mo _{0.97} (HfC) _{0.03} | 0.7% | 3.3% | - |
| Moo os (HfC)o os | _ | 5.5% | 4.2% |

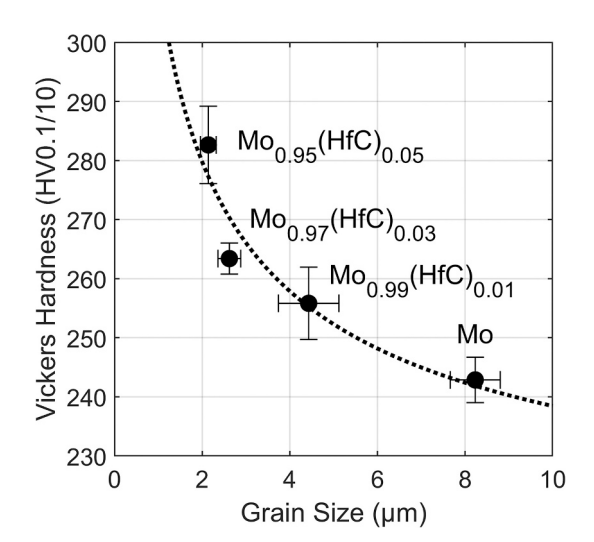


Fig. 7. Grain size as a function of increasing HfC faction, with Hall-Petch-like behavior overlaid. The error bars represent one standard deviation.

the value of HV_0 was 211 HV, while the constant k was 92 HV $\mu m^{1/2}$. These values are greater than those reported for pure molybdenum fabricated by powder metallurgy by Kim, who reported values of 159 HV and 53 HV $\mu m^{1/2}$, respectively, and the discrepancy is hypothesized to be attributed to additional hardening by the oxides and carbides and higher densities; Kim's density was between 90 and 93% [39].

3.2. Mechanical properties

In the bilinear constitutive models, the parameter σ_p is approximately constant regardless of added HfC, as shown in Fig. 8a, and all mechanical testing samples began behaving nonlinearly at approximately the same stress of 430 MPa. In comparison, the secondary slope, as shown in Fig. 8b, was nearly zero for the pure molybdenum and increased continuously with increasing HfC.

For each sample, the calibrated constitutive behavior is shown in in Fig. 8c, with curves terminating at the stress of the most highly stressed element at that sample's failure displacement. The local stress of the pure molybdenum samples does not exceed 500 MPa because of the embrittling effect of MoO₂, not meeting the strength requirement of 585 MPa for pure molybdenum produced by powder metallurgy [27]. For samples with added HfC, the stress at the outer fibers reached between 630 and 740 MPa. The failure strain was greatest for the Mo_{0.99}(HfC)_{0.01} samples, and increased addition of HfC reduced the failure strain.

SEM micrographs near the fracture surface of nominally pure molybdenum showed cracking between MoO₂ particles in Fig. 9a. These cracks were not located on the fracture surface and therefore dissipated energy without directly causing fracture. Additional microcracks may have closed upon elastic unloading during fracture and might not be visible. In Fig. 9b, cracking was observed in the samples with added HfC, forming networks between particles. The cracks were more tortuous than for the nominally pure molybdenum sample, and it is hypothesized that the HfO₂ particles initiated microcracking during deformation or

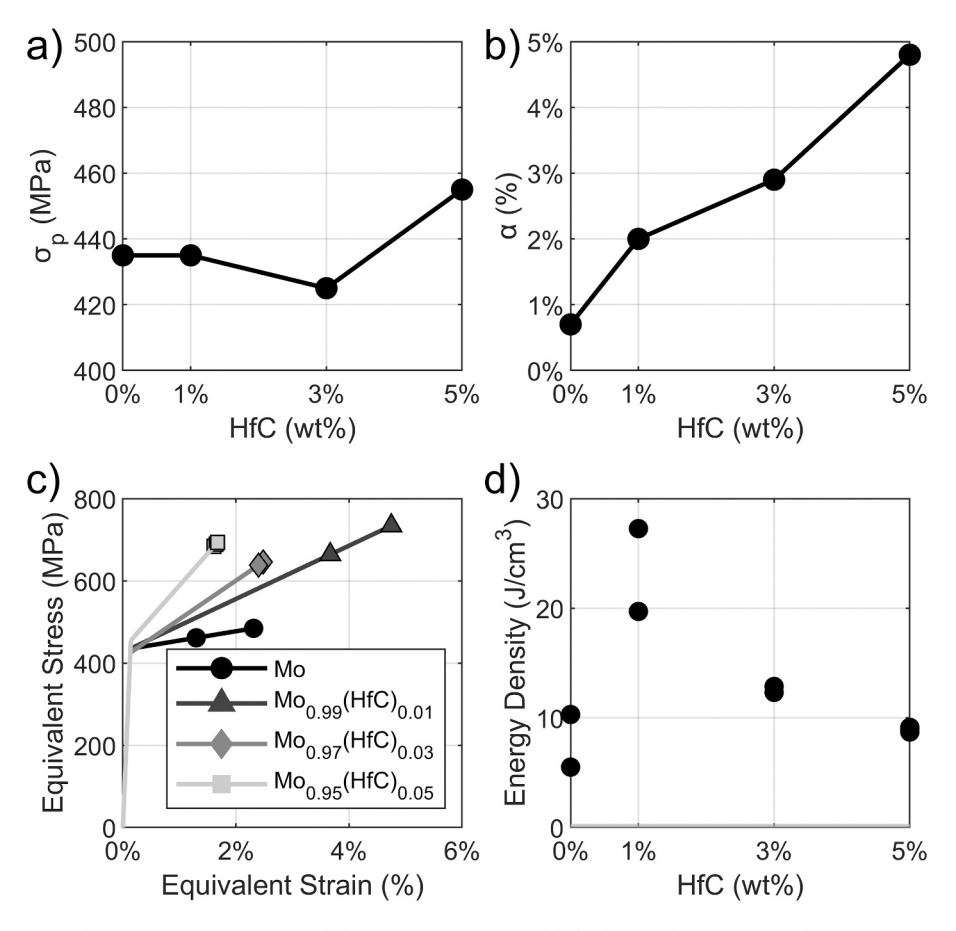


Fig. 8. Best-fit finite element simulation parameters, (a) σ_p and (b) α , as a function of added HfC. (c) The constitutive behavior of the compositions, in von Mises stress and total von Mises strain, where the markers correspond to the experimentally determined failure displacements. (d) Strain energy density of the most critical point on each sample at failure as a function of HfC.

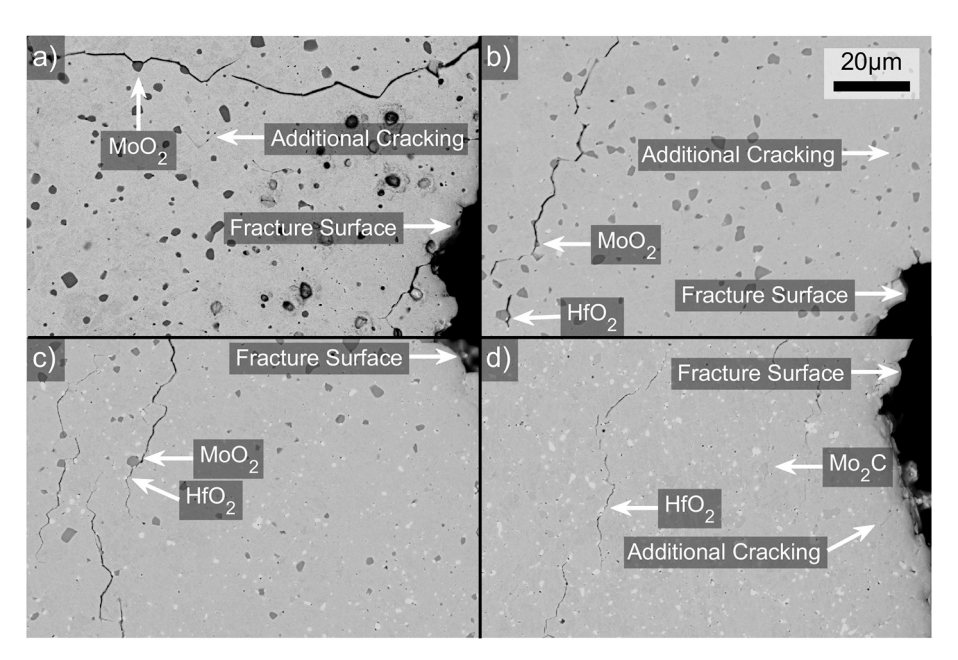


Fig. 9. SEM micrographs of regions near fracture surfaces, for the (a) nominally pure Mo, (b) $Mo_{0.99}HfC_{0.01}$, (c) $Mo_{0.97}HfC_{0.03}$, and (d) $Mo_{0.95}HfC_{0.05}$ samples. Cracks form between particles, and are more tortuous for samples containing more HfO_2 , implying that HfO_2 deflects cracks and contributes to increased strength and stiffness. Some smaller cracks are indicated with arrows.

during fabrication due to the tetragonal to monoclinic transformation. The presence of the preexisting microcracks around HfO_2 particles, or the nucleation of these microcracks during loading, would deflect cracking between MoO_2 particles during straining, thereby hindering crack coalescence. With increasing HfC added, the ratio of HfO_2 to MoO_2 grew and the ability to deflect – and thereby limit – crack growth increased, explaining the increasing parameter α (Fig. 8b). For the samples fabricated with 5% HfC, there was no MoO_2 , and the microcracks caused by HfO_2 alone resulted in a secondary slope approximately 5% of the modulus.

The volumetric energy density of material with a constitutive behavior described by bilinear stress-strain relationships is:

$$u_{bilinear} = \frac{\sigma_f^2 - \sigma_p^2 (1 - \alpha)}{2E\alpha}$$
 (5)

where σ_f is the failure stress. The energy absorption capability is shown in Fig. 8d. For comparison, if no crack arresting mechanisms were available and fracture occurred immediately at the material's nonlinearity, the energy absorption would be 0.3 J/cm³, which is between 18 and 93 times smaller than the observed energy absorption capability. The mechanism hypothesized to be microcracking increases the energy absorption capability by more than an order of magnitude. Compared to the nominally pure Mo, the addition of 1% HfC formed HfO2, reducing grain boundary oxygen and limiting MoO₂. Because the Mo_{0.99}(HfC)_{0.01} samples contained sufficient HfO2 particles to deflect crack growth but the greatest amount of MoO₂ particles for forming microcrack networks, it had the greatest room temperature energy absorption capability, while Mo_{0.97}(HfC)_{0.03} and Mo_{0.95}(HfC)_{0.05} had fewer MoO₂ particles and formed a less dense crack network, and failed at smaller strain energy densities. Compared to the Mo_{0.99}(HfC)_{0.01} samples, the Mo_{0.97}(HfC)_{0.03} and Mo_{0.95}(HfC)_{0.05} compositions had less grain boundary oxygen and MoO₂, but the mechanical strength did not improve, showing that only a small amount of HfO2 formation is required to limit the detrimental effect of oxygen.

4. Conclusions

The effect of oxygen on ODS and CDS molybdenum with added HfC was studied, and room-temperature mechanical behavior was linked to microstructure. This study's primary conclusions are:

- FAST was used to produce near theoretical dense Mo_{1-x}(HfC)_x samples without sintering aids, and HfC acted as a grain refiner, where greater amounts of HfC corresponded to smaller grains and increased microhardness.
- The presence of oxygen caused samples with 1 wt% and 3 wt% added HfC to form HfO₂ and MoO₂, while the samples with 5 wt% added HfC formed HfO₂ and Mo₂C.
- A bilinear material model was required to describe the measured mechanical behavior, indicative of an active toughening mechanism that was hypothesized to be microcracking. The addition of HfC had negligible effect on the stress of non-proportionality but significantly increased the slope after non-proportionality.
- The local failure stress of molybdenum without added HfC was limited by MoO₂ and did not exceed 500 MPa, while samples with added HfC were between 630 and 740 MPa.
- The composition of Mo_{0.99}(HfC)_{0.01} resulted in the greatest strain energy density prior to failure (20–30 J/cm³). The toughening mechanism was hypothesized to be microcracks between MoO₂ particles that were deflected by HfO₂ particles.

CRediT authorship contribution statement

Erik T. Furton: Formal analysis, Investigation, Validation, Data curation, Visualization, Writing – original draft. **Patrick E. Albert:**

Formal analysis, Investigation, Validation, Data curation, Writing – review & editing. **Dax H. Hoffman:** Formal analysis, Investigation, Validation, Data curation. **Douglas E. Wolfe:** Conceptualization, Methodology, Resources, Writing – review & editing, Project administration, Funding acquisition. **Allison M. Beese:** Conceptualization, Methodology, Supervision, Resources, Writing – review & editing, Project administration, Funding acquisition.

Declaration of Competing Interest

The authors declare that they have no known competing financial interests or personal relationships that could have appeared to influence the work reported in this paper.

Data availability

Data will be made available on request.

Acknowledgements

The financial support provided by the National Science Foundation through award number CMMI-1652575 and the National Science Foundation Graduate Research Fellowship under Grant No. DGE1255832 is gratefully acknowledged.

References

- [1] J.L. Johnson, Sintering of refractory metals, in: Sintering of Advanced Materials, 2010, pp. 356–388, https://doi.org/10.1533/9781845699949.3.356.
- [2] H. Walser, J.A. Shields, Traditional and Emerging Applications of Molybdenum Metal and Its Alloys, IMOA, Newsletter 1 (2007) 1–16.
- [3] D. Sziroczak, H. Smith, A review of design issues specific to hypersonic flight vehicles, Prog. Aerosp. Sci. 84 (2016) 1–28, https://doi.org/10.1016/j. paerosci.2016.04.001.
- [4] A.V. Levy, S.E. Bramer, The development of refractory sheet metal structures, SAE Trans 68 (1960) 352–366.
- [5] A. Kumar, B.L. Eyre, Grain boundary segregation and intergranular fracture in molybdenum, Proc. R. Soc. Lond. A 370 (1979) 431–458, https://doi.org/10.1098/ rspa_1980_0043
- [6] A.S. Wronski, A.A. Johnson, The deformation and fracture properties of polycrystalline molybdenum, Philos. Mag. 7 (1962) 213–227, https://doi.org/ 10.1080/14786436208211856.
- [7] P. Raffo, Thermomechanical Processing of Molybdenum-Hfanium-Carbon Alloys, NASA Technical Note. TN D-5645, 1970.
- [8] W.D. Klopp, P.L. Raffo, W.R. Witzke, Strengthening of molybdenum and tungsten alloys with HfC, J. Metals 23 (1971) 27–38, https://doi.org/10.1007/bf03355708.
- [9] L.L. Zhang, L.J. Zhang, J. Long, J. Ning, J.X. Zhang, S.J. Na, Effects of titanium on grain boundary strength in molybdenum laser weld bead and formation and strengthening mechanisms of brazing layer, Mater. Des. 169 (2019), https://doi. org/10.1016/j.matdes.2019.107681.
- [10] R. Liu, Z.M. Xie, T. Hao, Y. Zhou, X.P. Wang, Q.F. Fang, C.S. Liu, Fabricating high performance tungsten alloys through zirconium micro-alloying and nano-sized yttria dispersion strengthening, J. Nucl. Mater. 451 (2014) 35–39, https://doi.org/ 10.1016/j.jnucmat.2014.03.029.
- [11] T. Zhang, Z. Xie, J. Yang, T. Hao, C. Liu, The thermal stability of dispersion-strengthened tungsten as plasma-facing materials: a short review, Tungsten. 1 (2019) 187–197, https://doi.org/10.1007/s42864-019-00022-9.
- [12] W. Hu, Z. Du, Z. Dong, L. Yu, T. Ahamad, Z. Ma, The synthesis of TiC dispersed strengthened Mo alloy by freeze-drying technology and subsequent low temperature sintering, Scr. Mater. 198 (2021), https://doi.org/10.1016/j. scriptamat.2021.113831.
- [13] Z. Dong, Z. Ma, Y. Liu, Accelerated sintering of high-performance oxide dispersion strengthened alloy at low temperature, Acta Mater. 220 (2021), https://doi.org/ 10.1016/j.actamat.2021.117309.
- [14] Z. Dong, S. Chen, S. Liu, Z. Ma, L. Yu, Low-temperature accelerated sintering of high-performance oxide dispersion strengthened ultrafine grained Mo alloy, J. Alloys Compd. 903 (2022). https://doi.org/10.1016/j.jallcom.2022.163982.
- [15] Y. Kim, K.H. Lee, E.P. Kim, D.I. Cheong, S.H. Hong, Fabrication of high temperature oxides dispersion strengthened tungsten composites by spark plasma sintering process, Int. J. Refract. Met. Hard Mater. 27 (2009) 842–846, https://doi. org/10.1016/j.ijrmhm.2009.03.003.
- [16] S.-X. Yan, G.-D. Sun, J.-P. Xu, M.-Y. Li, J. Xu, F.-F. Wu, Y.-S. Zhang, In-situ oxide dispersion strengthened ultrafine-grained molybdenum alloy with enhanced hardness and bending strength, Mater. Today Commun. 105821 (2023), https:// doi.org/10.1016/j.mtcomm.2023.105821.
- [17] B.V. Cockeram, The fracture toughness and toughening mechanism of commercially available unalloyed molybdenum and oxide dispersion strengthened molybdenum with an equiaxed, large grain structure, Metall. Mater. Trans. A Phys.

- Metall. Mater. Sci. (2009) 2843–2860, https://doi.org/10.1007/s11661-009-9919-0
- [18] A.J. Mueller, R. Bianco, R.W. Buckman, Evaluation of oxide dispersion strengthened (ODS) molybdenum and molybdenum-rhenium alloys, Int. J. Refract. Met. Hard Mater. 18 (2000) 205–211, https://doi.org/10.1016/S0263-4368(00) 00028-7
- [19] A.G. Evans, Y. Fu, Some effects of microcracks on the mechanical properties of brittle solids-II. Microcrack toughening, Acta Metall. 33 (1985) 1525–1531, https://doi.org/10.1016/0001-6160(85)90053-7.
- [20] R.O. Ritchie, Mechanisms of Fatigue Crack Propagation in Metals, Ceramics and Composites: Role of Crack Tip Shielding, Mater. Sci. Eng. A. 103 (1988) 15–28, https://doi.org/10.1016/0025-5416(88)90547-2.
- [21] K.S. Hwang, H.S. Huang, The Liquid Phase Sintering of Molybdenum with Ni and Cu Additions, Mater. Chem. Phys. 67 (2001) 92–100, https://doi.org/10.1016/ S0254-0584(00)00425-9
- [22] E. Wuchina, E. Opila, M. Opeka, W. Fahrenholtz, I. Talmy, UHTCs: Ultra-high temperature ceramic materials for extreme environment applications, in: Electrochemical Society Interface 16, 2007, pp. 30–36, https://doi.org/10.1149/2. 604074if
- [23] O. Guillon, J. Gonzalez-Julian, B. Dargatz, T. Kessel, G. Schierning, J. R\u00e4thel, M. Herrmann, Field-assisted sintering technology/spark plasma sintering: mechanisms, materials, and technology developments, Adv. Eng. Mater. 16 (2014) 830–849, https://doi.org/10.1002/adem.201300409.
- [24] D.E. Wolfe, P.E. Albert, C.J. Ryan, J.A. Reiss, S.P. Stepanoff, P.A. Kolonin, Optimized processing of high density ternary hafnium-tantalum carbides via field assisted sintering technology for transition into hypersonic applications, J. Eur. Ceram. Soc. 42 (2022) 327–335, https://doi.org/10.1016/j. jeurceramsoc.2021.10.014.
- [25] R. Ohser-Wiedemann, U. Martin, H.J. Seifert, A. Müller, Densification behaviour of pure molybdenum powder by spark plasma sintering, Int. J. Refract. Met. Hard Mater. 28 (2010) 550–557, https://doi.org/10.1016/j.ijrmhm.2010.03.003.
- [26] B. Mouawad, M. Soueidan, D. FabrèGue, C. Buttay, V. Bley, B. Allard, H. Morel, Full densification of molybdenum powders using spark plasma sintering, Metall.

- Mater. Trans. A Phys. Metall. Mater. Sci. 43 (2012) 3402–3409, https://doi.org/ 10.1007/s11661-012-1144-2.
- [27] ASTM International, Standard Specification for Molybdenum and Molybdenum Alloy Bar, Rod, and Wire (B387/B387M - 23), 2023, https://doi.org/10.1520/ B0387 B0387M-23.
- [28] L.I. Emel'yanova, V.V. Rybin, Yu V. Solomko, Y.F. Titovets, Influence of carbon and oxygen impurities on the strength of molybdenum, Sov. Mater. Sci. 19 (1984) 496–499, https://doi.org/10.1007/BF00722113.
- [29] J. Wadsworth, J.P. Wittenauert. The History of Development of Molybdenum Alloys for Structural Applications, 1993.
- [30] L. Huang, Y. Pan, J. Zhang, Y. Du, F. Luo, S. Zhang, CALPHAD-type modeling of the C-Hf-Mo system over the whole composition and temperature ranges, Thermochim. Acta 692 (2020), https://doi.org/10.1016/j.tca.2020.178716.
- [31] ASTM International, Standard Test Methods for Determining Average Grain Size (E112-13), 2021, https://doi.org/10.1520/E0112-13R21.
- [32] ASTM International, Standard Test Method for Vickers Indentation Hardness of Advanced Ceramics (C1327 – 15), 2015, https://doi.org/10.1520/C1327-15R19.
- [33] ASTM International, Standard Test Method for Flexural Strength of Advanced Ceramics at Ambient Temperature, Annual Book of ASTM Standards (C1161-18), 2018, pp. 1–16, https://doi.org/10.1520/C1161-18R23.
- [34] J.R. Davis, Metals Handbook Desk Edition, Second Edition, 1998.
- [35] T.L. Anderson, Fracture Mechanics: Fundamentals and Applications, Fourth Edition, 2017.
- [36] J. Wang, H.P. Li, R. Stevens, Hafnia and hafnia-toughened ceramics, J. Mater. Sci. 27 (1992) 5397–5430, https://doi.org/10.1007/BF00541601.
- [37] E.O. Hall, The deformation and ageing of mild steel: III discussion of results, Proc. Phys. Soc. Sect. B 64 (1951) 747–753, https://doi.org/10.1088/0370-1301/64/9/303.
- [38] N.J. Petch, The cleavage strength of polycrystals, J. Iron Steel Instit. 174 (1953) 25–28.
- [39] Y. Kim, Consolidation behavior and hardness of P/M molybdenum, Powder Technol. 186 (2008) 213–217, https://doi.org/10.1016/j.powtec.2007.12.005.